Approaches for Astrometry using Event-Based Sensors

Gregory Cohen, Saeed Afshar, and André van Schaik
The MARCS Institute for Brain, Behavior and Development
Western Sydney University, Sydney, Australia

ABSTRACT

Event-based sensors are novel optical imaging devices that offer a different paradigm in which to image space and resident space objects. Also known as silicon retinas, these custom silicon devices make use of independent and asynchronous pixels which produce data in the form of events generated in response to changes in log-illumination rather than in the conventional frames produced by CCD-based imaging sensors. This removes the need for fixed exposure times and frame rates but requires new approaches to processing and interpreting the spatio-temporal data produced by these sensors. The individual nature of each pixel also yields a very high dynamic range, and the asynchronous operation provides a high temporal resolution. These characteristics make event-based cameras well suited to terrestrial and orbital space situational awareness tasks.

Our previous work with these sensors highlighted the applicability of these devices for detecting and tracking resident space objects from LEO to GEO orbital regimes, both during the night and daytime without modification to the camera or optics. Building upon this previous work in applying these artificial vision systems to space situational awareness tasks, we present a study into approaches for calculating astrometry from the event-based data generated with these devices. The continuous nature of these devices, and their ability to image whilst moving, allows for new and computationally efficient approaches to astrometry, applicable both to high-speed tracking from terrestrial sensors and low-power imaging from orbital platforms.

Using data collected during multiple sets of telescope trials involving co-collections between a conventional sensor and multiple event-based sensors, a system capable of identifying stars and positional information whilst simultaneously tracking an object is presented. Two new prototype event-based sensors, offering increased spatial resolution and higher sensitivity, were also used and characterized in the trial, and updated observation results from these improved sensors are presented. These results further demonstrate and validate the applicability and opportunities offered by event-based sensors for space situational awareness and orbital applications.

1. INTRODUCTION

Event-based sensing represent a novel imaging paradigm for space imaging and offers the potential to overcome many of the problems plaguing conventional optical astronomy imaging systems. The unique in-pixel circuitry in event-based cameras coupled with the asynchronous and independent nature of each pixel in the array allows for high-speed, low-power, and high dynamic range imaging. Our prior work has demonstrated that event-based sensors offer the potential to detect resident space objects in a wide range of orbital regimes and in both daytime and nocturnal conditions [1]. Additonally, we have also began to explore tracking and detection algorithms for event-based systems [2] which serve to further highlight the potential for this technology.

This paper builds upon those two prior publications by addressing the task of astrometry with an event-based sensor As these sensors produce data as a stream of spatio-temporal information rather than conventional frames, existing techniques for astrometry are not directly applicable, and this paper explores techniques to generate star maps from an event-based sensor and then to use those star maps to determine the portion of the sky visible. The ability to visualize stars with an event-based camera is a critically important step in improving the usability and applicability of event-based cameras for optical astronomy and is required for future tasks such as calibrating the sensor and building pointing models using only an event-based sensor.

This paper examines the generation of star maps from an event-based camera pointed at a fixed spot on the geo-belt. Whilst this work explores the star map generation from a stationary event-based camera, the concepts and algorithms can be extended to cover the case of a moving camera. This is an important building block in the development of real-

time and continuous in-frame astrometry systems that can determine accurate references whilst the telescope is moving.

2. NEUROMORPHIC VISION SENSORS

This work makes use of a novel class of imaging devices which draw inspiration from biology and function more like a biological retina than a conventional camera. These devices fall neatly into the original definition of neuromorphic engineering as they attempt to model neuro-biology through the use of electronic and silicon-based design. The term neuromorphic has since been expanded in scope to include a range of biologically-inspired systems implemented using analogue, digital, and mixed-signal hardware [3]. The class of imaging devices used in this work are referred to event-based silicon retinas or Dynamic Vision Sensors (DVS). There exist a number of different prototype silicon retinas, and this work will refer to them collectively as event-based cameras.

Event-based cameras have been developed to more closely resemble, at a hardware level, the operation of vision systems in nature [4]. These sensors are composed of an array of specialized pixels which respond independently and asynchronously to changes in the scene. Unlike a typical CCD or CMOS framing camera, the devices do not produce "images" or "frames" at a fixed rate, but rather produces a continuous stream of spatio-temporal events in response to changes in the scene. This removes the need for fixed exposure times, which, combined with in-pixel logarithmic compression, provides the devices with a very high dynamic range (up to 140dB) [5] and allows for continuous frame-free sky imaging.

These devices are inherently low power and have a high temporal resolution, capable of generating events with microsecond timing from each pixel. This is accomplished using specialized in-pixel circuitry and an asynchronous readout mechanism, both of which enable high-speed tracking applications and allow for extremely accurate orbital range calculations across multiple sensors. In stark contrast to conventional sensors, the high-speed operation allows movement to enhance the performance of these sensors, instead of creating motion blur. This therefore creates new and unique imaging opportunities and applications. Event-based cameras therefore provide an avenue to potentially reduce data bandwidth, to improve dynamic range, and to reduce power requirements – all of which are of particular importance to space situational awareness systems, both terrestrially and in-orbit.

The primary output of an event-based camera can be viewed as a continuous stream of events $\boldsymbol{e}$, each of which have the following form [6]:

$$\boldsymbol{e} = [x, y, p, t]^{\boldsymbol{T}}$$

In which $\boldsymbol{u} = [x, y]$ denotes the location of the pixel generating the event, $p \in \{-1, +1\}$ indicates the polarity of the change in illumination at the pixel causing the event, and t represents the time at which the event occurred. In a true event-based system, the time would be implicit in the arrival time of the event, but to preserve the timing when saving data from the camera, a time stamp is applied by the camera hardware as the event is generated. For both cameras, the timestamps are stored with microsecond resolution. This output method is directly compatible with the Address-Event Representation (AER) [7] that is commonly used in neuromorphic engineering and neuromorphic cognition systems.

This output stream is similar to a photon counting imager (PCI) based on a photocathode front-end, multi-channel plates for electron multiplication, and a readout anode to enable detection of the position and time of each detected photo-electron. However, the event-based cameras are entirely solid state and therefore tend to be much more compact devices, and do not face the same dynamic range issues of PCIs due to the sensing of changes in flux as opposed to the flux itself.

It should also be noted that most event-based cameras include additional circuitry to provide some measure of absolute illumination. This auxiliary output differs between cameras and is often used to verify that the devices are functioning and to simplify the process of calibration. The absolute illumination outputs often suffer from the same set of problems plaguing frame-based imaging devices and therefore are not used in this work.

This paper expands on our previously published event-based space imaging work by making use of four different event-based silicon retinas. In addition to the DAVIS240C and the ATIS camera used in the previous set of experiments, this work also makes use of the next generation prototypes of those sensors. These devices, the DAVIS346 BSI and the ATIS640, improve on the pixel density of the original cameras and provide significantly

higher resolution. The DAVIS346 camera is also unique in that it was produced using a back-illuminated silicon process [8], resulting in a highly sensitive sensor with a very high quantum efficiency. To date, our work represents the only use of these devices for space imaging tasks.

Table 1: Characteristics and physical properties of the commonly used event-based neuromorphic sensors.

Parameter	**DAVIS240C** [9]	**ATIS** [5]	**DAVIS346 BSI** [8]	**ATIS640***
Pixels	240 x 180 (DVS) 240 x 180 (APS)	304 x 240 (DVS) 304 x 240 (APS)	346 x 240 (DVS) 346 x 240 (APS)	640 x 480 (DVS) DVS Only
Power consumption	5mW–14mW	50mW–175mW	5mW–14mW	Not known
Dynamic Range	130 dB	125 dB	130 dB	120 dB
Chip Size	5mm x 5mm	9.9mm x 8.2mm	5mm x 5mm	9.9mm x 8.2mm
CMOS Technology	18µm 6M 1P	18µm 6M 1P	18µm 6M 1P	0.20µm 6M 1P
Fill factor	22%	20% TD, 10% EM	22%	Not known
Pixel Size	18µm x 18µm	30µm x 30µm	18µm x 18µm	20µm x 20µm

* Estimated values. Device used was an early prototype stage and accurate data was not available.

Table 1 provides the physical properties and characteristics of four different event-based neuromorphic sensors used in this work. In addition to the ATIS and DAVIS240C devices used in our previous work, the table also includes the next generation prototypes of both sensors. These new generation sensors have increased pixel density, better power consumption, and higher fill factors. The ATIS and DAVIS240C cameras are the most mature of the event-based devices and are the most widely available and widely used devices, whereas the DAVIS346 BSI variant exists as a single working prototype. In a similar fashion. the ATIS640 camera is an early prototype of a full VGA camera variant, and as a result many of the technical characteristics have not been provided or determined.

3. EXPERIMENTAL SETUP

This paper makes use of data collected from two different sets of telescope field trials conducted with Defence Science and Technology (DST) in South Australia. The optical telescopes and mounts are the same ones used in our prior publications on event-based space imaging, although the configuration and optical assemblies were changed for some of the later experiments. An overview of the equipment used in these experiments is shown in Figure 1.

The experiments were all conducted using a similar methodology in which the event-based cameras are in co-located and bore-sighted alongside a standard astronomy camera. The astronomy camera, an FLI Proline PL47010 camera, is used to provide ground truth and used to build an accurate mount model, allowing the event-based cameras to be accurately pointed at celestial objects. The telescopes are mounted on a Software Bisque Paramount MEII robotic mount. The entire system has been installed in a 7ft Aphelion Dome mounted on a standard vehicle trailer, as shown in Figure 1 (b).

(a) (b) (c)

Figure 1: Photographs of the equipment used to capture the data used for star mapping. The above images show the hardware used to capture the data used in this paper. The data was captured over two different sets of telescope trials conducted in collaboration with Defence Science and Technology (DST) in Edinburgh and Woolmera in South Australia. Both experiments made use of a mobile telescope configuration consisting of three co-mounted and bore-sited telescopes on a robotic mount. The initial configuration consisting of two 8'' Meade LX200 telescopes and a single Officina Stellare RH200 is shown in (a) and was used in the first sets of experiments with a static camera. Further experiments were conducted using the configuration shown in (c),

in which two Officina Stellare RH200s were co-located with a single 8'' Meade LX200. The entire platform is housed in a movable dome installed on a standard vehicle trailer, as shown in (b).

The experiments were performed using two different configurations of optical telescopes. The first configuration made use of two 8" Meade LX200 telescopes bore-sighted alongside an Officina Stellare RH200 telescope on which the ground truth camera was installed. This configuration is shown in Figure 1 (a), and the DAVIS240C camera can be seen installed on the top telescope, with the ATIS camera installed on the lower camera. The second configuration made use of the same mount and ground-truth optical assembly but included a second Officina Stellare RH200 telescope instead of two 8'' Meade LX200s. This configuration is shown in Figure 1 (c) with the DAVIS346 BSI sensor visible on the left telescope and the ATIS640 visible on the telescope on the right.

The experiments were carried out during multiple field trials occurring in Edinburgh, South Australia and in the Woolmera in South Australia.

4. ASTROMETRY WITH A STATIC EVENT-BASED CAMERA

Tackling the task of figuring out the location of the field of view within the night sky with an event-based camera, required the development of new algorithms and techniques to produce conventional images of the sky using the data from an event-based camera. These algorithms therefore generate images that are compatible with sky catalogue software and can allow for the use those databases to locate and identify the star map. In future, this work will be expanded to operate entirely in an event-based paradigm, but this would require creating new event-based star catalogues derived from the existing star catalogues. Although this is a future direction for this research, this paper focuses on the task of identification through the use of conventional and widely available astrometry software and systems.

The experiments reported in this paper make use of data recorded whilst the telescope was staring at a fixed point on the geo-belt. For the results presented in this section, the telescope was pointed at the Optus D2 satellite. The telescope therefore was not tracking and remained immobile, removing any events generated by motion of the telescope. Therefore, the only source of change events arises from objects moving in the field of view and from inherent noise in the sensor. As the telescope is static, the stars therefore move through the field of view at a constant velocity as a result of the rotation of the earth. Given the distance to the stars, we can make the assumption that rotation at that distance is well approximated as a pure translation on the sensor surface.

The method used to create the star map from the event-based camera output was originally inspired and adapted from methods to perform real-time and simultaneous mosaicing with event-based cameras [10]**.** Although this method formed the starting point for this research, there are several simplifications that can be made in order to apply a similar technique to space imaging. For consistency, we have made use of their notation. We can then use the following equations to convert from camera coordinates, $\boldsymbol{p_c} = \boldsymbol{u} = [x, y]$ to sky coordinates $\boldsymbol{P_m}$ as follows:

$$\boldsymbol{P_m} = \boldsymbol{P_c} - \boldsymbol{v_c}(t)$$

In the above equation, $\boldsymbol{P_m} = [x, y]^T$ denotes the denotes the mapped coordinates on the star field for the given event $\boldsymbol{e}$ generated from pixel $\boldsymbol{P_c} = [u, v]^T$ in the camera at time $\boldsymbol{t}$. The velocity function $\boldsymbol{v_c}(t)$ represents the motion of the camera as a function of time. When the telescope is static and staring, the velocity function becomes a constant function of $\boldsymbol{t}$ as follows:

$$v_c(t) = \begin{bmatrix} v_x t \\ v_y t \end{bmatrix}^T$$

Under the pure rotation assumption when staring with the telescope, the constants v_x and v_y are determined by the pixel size, pixel and the field of view. For the DAVIS camera, the camera has a pixel array of 240×180 18 μm pixels and attached to a telescope with a 2000 mm focal length. This yields a field of view of approximately 7.44×5.58 arc mins, or 0.124×0.093 degrees. We can therefore estimate the velocity of a star crossing the field of view as $v_x = v_y = 8.0645$ pixels per second.

We determined the velocities manually by tracking stars at they crossed the field of view. This was undertaken as there were alignment issues with the sensor resulting in the being tilted relative to the ground truth sensor and therefore the mount model. Through tracking multiple stars in the recording and averaging their velocity across the sensor surface, the following values of v_x and v_y were determined:

$$v_c(t) = \begin{bmatrix} v_x t \\ v_y t \end{bmatrix}^T = \begin{bmatrix} -1.2689t \\ -7.1284t \end{bmatrix}^T$$

Note that the negative values for v_x and v_y arise from the alignment of the camera on the telescope and the direction in which the pixels are assigned addresses on the sensor.

In order to generate a star map, the events from the camera need to be converted to camera space using the above equations and then accumulated. The inherent assumption is that any star moving through the field of view will be mapped to the same point on the sky, whereas noise will be distributed across the sky field. Fixed pattern noise on the sensor, arising from pixels with higher than average firing rates, will distributed across the sky map with a predictable distribution. As a result, the star map can then be generated by taking the accumulated star map and thresholding it against the mean event rate.

An example of a star map generated using the above method is presented in Figure 2. The figure shows a star map generated by the DAVIS240 sensor whilst staring at an object in the GEO belt. By converting each event from camera coordinates to sky coordinates and accumulating them, the star map show in Figure 2 can be generated.

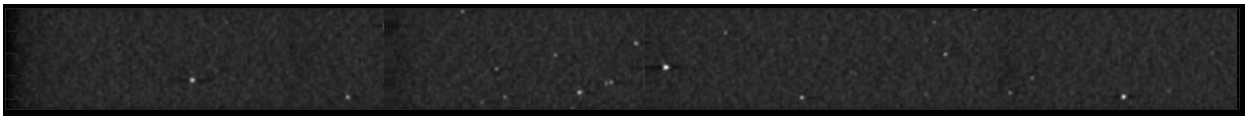

Figure 2: Star map generated from an event-based camera. The above image represents a star map generated from an event-based camera staring at Optus C1. The recording was made over 420 seconds with no sidereal tracking.

The star map generated in Figure 1 was recorded over a period of 420 seconds. Although the rotation of the earth was used to generate the motion across the sensor surface, it is entirely possible to actively move the telescope and create star maps much faster as long as the nature of the motion is known. Most robotic telescope mounts are well suited to providing such information about the motion as they comprise highly calibrated and accurate motors and can be used to build accurate pointing models to further calibrate the device.

The generated star map was then aligned to a ground truth image obtained from the astronomy camera. This is presented in Figure 3 with the event-based star map inset underneath a rectangle showing where the two images align. It is important to note that the event-based camera has a much narrower field of view when compared to the CCD imager used to obtain the ground truth images. The astronomy camera used has a resolution of 2048 x 2048 pixels and was attached to the Officina Stellare telescope which has a wider field of view. By comparison, the event-based camera was attached to an 8'' Meade telescope and has a pixel resolution of only 240 x 180 pixels.

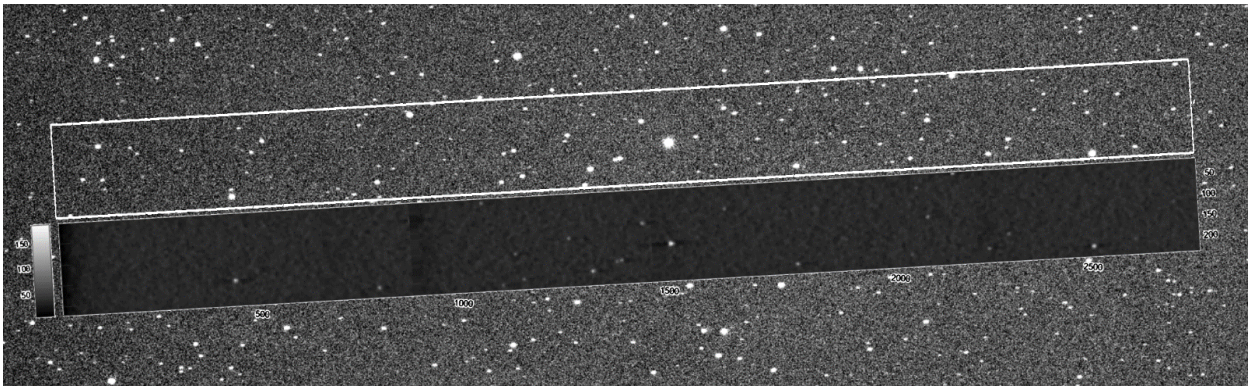

Figure 3: A star map generated by the event-based camera and overlaid over the ground truth CCD image. The star map generated by the event-based camera is shown as the inset in the above image. Above the inset, the correct location on the ground-

truth image is shown within the white rectangle. Through the correct estimation of the velocity, the generated star map did not require any scaling or distortion in order to line up with the ground truth image. Note that the slight rotation is a result of a misalignment between the event-based camera and the astronomy CCD camera.

In order to further validate the effectiveness of the star mapping process, the two images were then processed using Astrometry.net to determine the sky location from the images alone. The results of the astrometry calculations are shown in Figure 4 with the relevant astrometry information provided in **Table 2**.

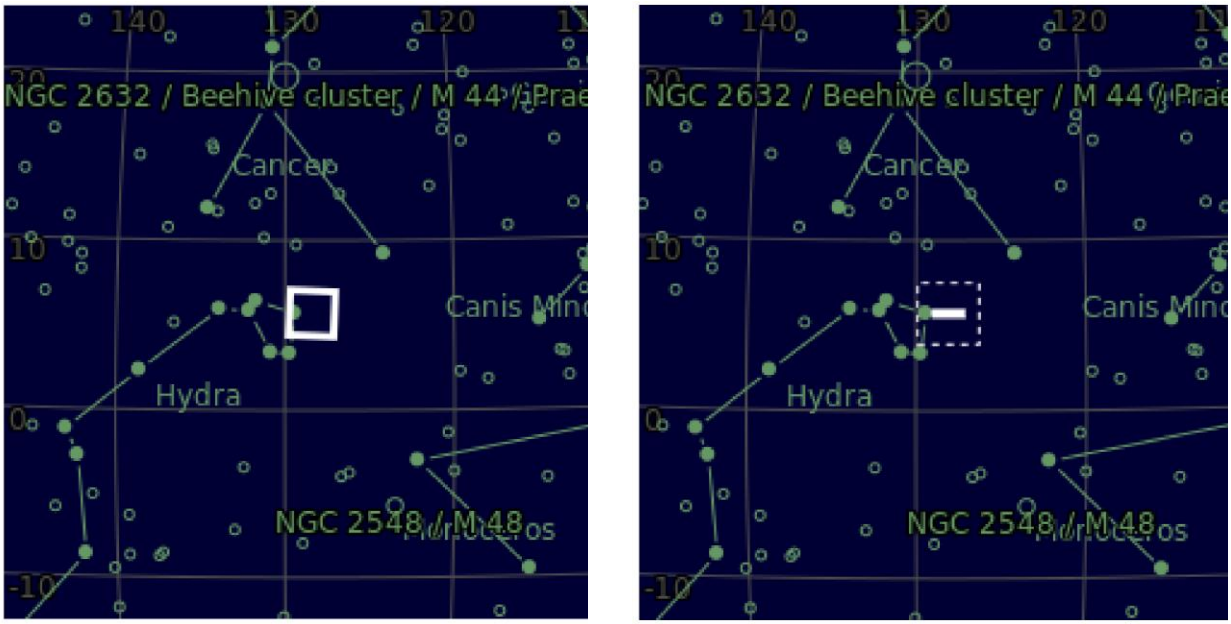

Ground-truth location
(a)

Event-based Star Map Location
(b)

Figure 4: Comparison of sky locations computed from the two cameras. The sky location found using the ground truth camera is shown in (a) and the sky location calculated using the event-based camera is shown in (b). Note that the field of views of the two cameras accurately match the size of the images generated, with the astrometry camera mapping to a square region on the sensor, whilst the event-based sensor generated an elongated rectangle.

The results show that the star mapping technique can generate images that successfully matched the sky location. The shape and size of the two fields of view are consistent with the size and shape of the images generated by both the event-based camera and the ground-truth camera.

Ground-truth Camera Astrometry	
Centre (RA, Dec):	(128.399, 5.714)
Centre (RA, hms):	08h 33m 35.666s
Centre (Dec, dms):	+05° 42' 50.152"
Size:	2.64 x 2.64 deg
Radius	1.865 deg
Pixel Scale	4.64 arcsec/pixel

DVS Camera Astrometry	
Centre (RA, Dec):	(128.103, 5.708)
Centre (RA, hms):	08h 32m 24.790s
Centre (Dec, dms):	+05° 42' 28.466"
Size:	95.4 x 8.52 arcmin
Radius	0.798 deg
Pixel Scale	4.65 arcsec/pixel

Table 2: Astrometry results from the ground truth camera and from the DVS camera.

The results produced with the star mapping process serve to successfully demonstrate and validate the use of event-based cameras for star tracking and star mapping techniques. The techniques and algorithms used to generate the star maps are not computationally expensive and lend themselves well to implementation on a small microcontroller platform, making them well suited to the size, weight, and power restrictions of a small satellite platform.

5. CONCLUSIONS

The work in this paper serves to demonstrate the viability of using event-based sensors for real-time and continuous astrometry. This was accomplished through the generation of sky images from the event-based data for use with conventional astrometry software. It is also important to note that the event-based sensors will still detect fast-moving objects, such as objects in low earth orbit, whilst generating the star map as the two processes are independent of one another. This work therefore represents an important building block towards building real-time and continuous event-based astrometry systems, with future work exploring the generation of star maps whilst the telescope is actively moving. Future work will also seek to perform the astrometry in a real-time and continuous manner without resorting to intermediate image generation. However, the immediate benefit to the approach described in this paper is the potential for integration into existing optical telescopes and processing systems.

6. REFERENCES

[1] G. Cohen, S. Afshar, A. Schaik, A. Wabnitz, T. Bessel, M. Rutten and B. Morreale, "Event-based Sensing for Space Situational Awareness," in *Advanced Maui Optical and Space Surveillance Technologies Conference (AMOS)*, 2017.

[2] B. Cheung, M. Rutten, S. Davey and G. Cohen, "Probabilistic Multi Hypothesis Tracker for an Event Based Sensor," in *Proceedings of the 21st International Conference on Information Fusion*, 2018.

[3] G. Indiveri and T. K. Horiuchi, *Frontiers in neuromorphic engineering,* vol. 5, 2011, pp. 1-2.

[4] T. Delbrück, B. Linares-Barranco, E. Culurciello and C. Posch, "Activity-driven, event-based vision sensors," in *Proceedings of 2010 IEEE International Symposium on Circuits and Systems*, 2010.

[5] C. Posch, D. Matolin and R. Wohlgenannt, "A QVGA 143 dB Dynamic Range Frame-Free PWM Image Sensor With Lossless Pixel-Level Video Compression and Time-Domain CDS," *IEEE Journal of Solid-State Circuits,* vol. 46, pp. 259-275, 1 2011.

[6] X. Lagorce, C. Meyer, S.-H. Ieng, D. Filliat and R. Benosman, "Asynchronous Event-Based Multikernel Algorithm for High-Speed Visual Features Tracking.," *IEEE transactions on neural networks and learning systems,* pp. 1-12, 9 2014.

[7] K. Boahen, "Point-to-point connectivity between neuromorphic chips using address events," *IEEE Transactions on Circuits and Systems II: Analog and Digital Signal Processing,* vol. 47, pp. 416-434, 5 2000.

[8] G. Taverni, D. Paul Moeys, C. Li, C. Cavaco, V. Motsnyi, D. San Segundo Bello and T. Delbruck, "Front and back illuminated dynamic and active pixel vision sensors comparison," *IEEE Transactions on Circuits and Systems II: Express Briefs,* vol. 65, no. 5, pp. 677-681, 2018.

[9] C. Brandli, R. Berner, M. Yang, S.-C. Liu and T. Delbruck, "A 240 x 180 130 dB 3 us Latency Global Shutter Spatiotemporal Vision Sensor," *IEEE Journal of Solid-State Circuits,* vol. 49, pp. 2333-2341, 10 2014.

[10] H. Kim, A. Handa, R. Benosman, S. H. Ieng and A. J. Davison, "Simultaneous Mosaicing and Tracking with an Event Camera," in *BMVC*, 2014.